

## STUDY OF THE EFFECT OF DIFFERENT INDUSTRIAL COATING WITH MICROSCALE THICKNESS ON THE CK45 STEEL BY EXPERIMENTAL AND FINITE ELEMENT METHODS

K. R. Kashyzadeh<sup>1</sup> and A. Arghavan<sup>2</sup>

UDC 539.4

*This article is aimed at analyzing the effects of industrial coatings of hardened chromium, trim chromium, hardened nickel and warm-galvanization with a thin structure and dimensions in micron scale, on fatigue endurance limit of components. In order to do this, using the plating process and the analyzed coatings with the thickness of 13 and 19  $\mu\text{m}$  under the operation conditions, the components of CK45 steel were plated. An attempt was made to analyze the fatigue of components by modeling the interface phase between the base metal and coating more accurately, using the linear spring elements. The  $S-N$  curves obtained via the proposed finite element model (including 3 different phases) and other finite element models in which the shell element was used to model the intermediate phase, are compared to the experimental results. The findings indicate that, considering the difference between the  $S-N$  curves constructed via the present finite element model and via test results, this model is improved in comparison to the earlier one, and yields more reliable results. Taking into account the environmental and operating conditions of components, the galvanized coating is the most appropriate among low-thickness coatings, but with significant increase in coating thickness, the best choice becomes hardened chromium coating. Increase in coating thickness by 6  $\mu\text{m}$  reduces the fatigue limit by 14.96 and 4.37% for galvanized and hardened chromium coatings, respectively.*

**Keywords:** fatigue, coating, hardened chromium, galvanized, trim chromium, hardened nickel,  $S-N$  curve, finite element model, intermediate phase.

**Introduction.** Under frequent and repeated tension, metal is broken by tensile stress, which is lower than the one required for fracture under static tension conditions. On the other hand, damage of component subjected to simultaneous action of fatigue and corrosion is much higher than that under consequent application of fatigue and corrosion conditions. In the latter situation, there is no clear change in the metal structure broken due to fatigue, which could be used as an evidence for recognition of the reasons of fatigue fracture. At least 90% of in-service component failures due to mechanical factors are caused by fatigue [1].

According to the standards of fatigue testing presented by the Association of Mechanical Engineers of Japan in 1981 and by ASTM in 1998 for constructing an  $S-N$  curve with the minimum number of test specimens, 14 test specimens are needed, 8 of which are used to determine the limited fatigue life values above the fatigue limit. Testing of two specimens at each of of four levels specifies the balance of the applied load. Also, the fatigue limit can be obtained by step-wise procedure with 6 test specimens.

Step-wise procedure, which is often referred to as the up-and-down method, is one of the most common ways that is consistent with most of the available criteria for evaluating the statistical properties of the fatigue limit [2, 3].

---

Islamic Azad University, Semnan, Iran (<sup>1</sup>kazem.kashyzadeh@gmail.com; <sup>2</sup>AlirezaArghavan@semnaniau.ac.ir). Translated from Problemy Prochnosti, No. 6, pp. 152 – 163, November – December, 2013. Original article submitted February 14, 2013.



Fig. 1. Tensile testing machine.

## 1. Obtaining the Mechanical Properties of the Components.

**1.1. Preparing the Components.** Ten cylindrical rod-shaped specimens of 12 mm in diameter and the length of 279 mm with the base metal CK45 are produced, according to tensile test standards, machined and subjected to surface treatment [4] for further deposition of each group of coatings under study.

At the final stage of preparation, analyzed coatings of various thickness are deposited under the same operation conditions, such as temperature, humidity and other factors [5].

**1.2. Testing Conditions.** In this study, tensile testing machine STM-600 is used in accordance with Fig. 1.

**1.3. Results.** The stress–strain curves obtained from tensile tests for components with different coatings (industrial coatings under study) of 13 and 19  $\mu\text{m}$  in thickness are depicted in Fig. 2. In Tables 1 and 2, the mechanical characteristics of the components with coatings of 13 and 19  $\mu\text{m}$  in thickness obtained from tensile test are tabulated, respectively.

## 2. Preparation of Components for Fatigue Tests.

**2.1. Number of Components Required.** As it was mentioned earlier, according to the ASTM standard in 1998, the number of experimental components required to get the first component of the  $S-N$  curve (limited lifetime above the fatigue limit) is equal to 8 specimens, however, in order to obtain more reliable results, 12 components have been used in experiment with 4 levels of applied cyclic load, 3 specimens being tested at each cyclic load level, so that the average fatigue life of 3 specimens is treated as the fatigue life at the respective cyclic load level.

**2.2. The Test Conditions.** Components for each group of analyzed coatings were made from CK45 steel according to the British Standard BS3518 for conducting fatigue tests, which specifies the recommended manufacturing methods for test specimens [7]. Test specimens with dimensions depicted in Fig. 3 are machined and subjected to surface treatment, and as the final step, the surface of specimens are polished by sandpaper No.600. The direction of polishing is along the length of the component, in order to minimize the surface roughness and make it smooth and glossy [4, 7].

It is noteworthy that, in order to reduce the error percentage at the stage of preparing the components, they have been subjected to rasping surface treatment, whereas dimensions of the blunt cones in the component edges described in Fig. 3 are controlled by Eq. (1):

$$\tan(\alpha/2) = \frac{D - d}{2L}, \quad (1)$$

where  $D$  is the larger-edge diameter of the blunt cone,  $d$  is its smaller-edge diameter, and  $L$  is the blunt cone length.

At the next stage, using the process of plating, the analyzed coatings with the thickness of 13 and 19  $\mu\text{m}$  have been deposited under the same operation conditions, including temperature, humidity and other factors effective in the components [8].

Using the scanning electronic microscope (SEM), several photos with magnification of 1000 were taken, as it is shown in Fig. 4, in order to analyze the accuracy of plating of components and the thickness of coatings.

TABLE 1. Mechanical Properties of Components with a Thickness of 13  $\mu\text{m}$  [6]

Result	Embellished chromium			Hardened chromium		
	Peak	Break	Yield	Peak	Break	Yield
Force (N)	105392.9	87833.47	105193.9	107045.3	95098.09	106539.9
Extension (mm)	1.810215	5.641043	1.478078	3.583356	6.912126	1.8323570
Stress (MPa)	931.8779	776.6183	930.1183	946.4883	840.8517	942.0194
Elongation	3.62043	11.28209	2.956157	7.166711	13.82425	3.664713
Elongation after break	3.457021	11.10079	2.792546	7.465292	13.8729	3.952722
Module (MPa)	25739.43	6883.641	31463.77	13206.73	6082.439	25705.13
Energy (kJ)	178.4	560.6	143.5	373.3	719.5	186.1
	Hardened nickel			Warm galvanizing		
Force (N)	110237.8	94113.62	109983.8	110415.8	95250.06	109962.8
Extension (mm)	0.5746964	3.280554	0.3065699	3.450773	7.622701	1.608388
Stress (MPa)	974.7166	832.1472	972.4702	976.2899	842.1954	972.2845
Elongation	1.149393	6.561108	0.6131397	6.901545	15.2454	3.216776
Elongation after break	1.053799	6.477806	0.5177394	6.904699	15.21457	3.218915
Module (MPa)	84802.73	12683.03	158605.0	14145.96	5524.259	30225.44
Energy (kJ)	96.3	377.4	43.1	376.7	821.2	173.6

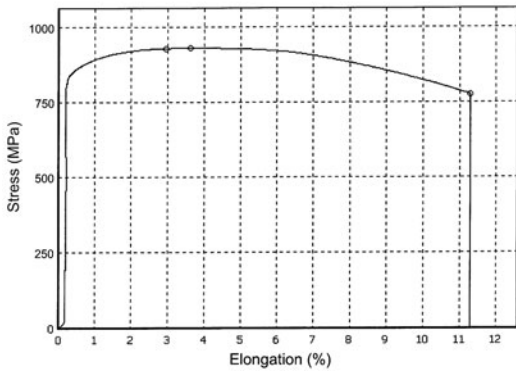
TABLE 2. Mechanical Properties of Components with a Thickness of 19  $\mu\text{m}$  [6]

Result	Embellished chromium			Hardened chromium		
	Peak	Break	Yield	Peak	Break	Yield
Force (N)	103591.1	86814.84	103509.9	105971.7	97161.85	105877.5
Extension (mm)	3.000181	6.830809	2.12211	0.1070035	0.055746	0.0906766
Stress (MPa)	915.9464	767.6118	915.2288	936.9957	859.0994	936.1623
Elongation	6.000362	13.66162	4.244219	0.214007	0.1114921	0.1813531
Elongation after break	5.589775	13.18036	3.83329	0.1689866	0.0685821	0.1363553
Module (MPa)	15264.85	5618.747	21564.12	437834.2	770547.6	516209.6
Energy (kJ)	289.8	666.7	198.8	273.0	203.0	249.0
	Hardened nickel			Warm galvanizing		
Force (N)	105175.5	92869.51	104662.2	106726.0	89014.71	106597.7
Extension (mm)	5.002722	9.035047	3.14964	0.5088025	4.231294	0.4345179
Stress (MPa)	929.9554	821.1467	925.4175	943.665	787.0629	942.5307
Elongation	10.00544	18.07009	6.299279	1.017605	8.462587	0.8690357
Elongation after break	9.98278	18.03479	6.276088	0.804564	8.260647	0.6560751
Module (MPa)	9294.494	4544.231	14690.85	92733.91	9300.499	108457.1
Energy (J)	520.5	933.7	325.9	56.0	431.2	48.1

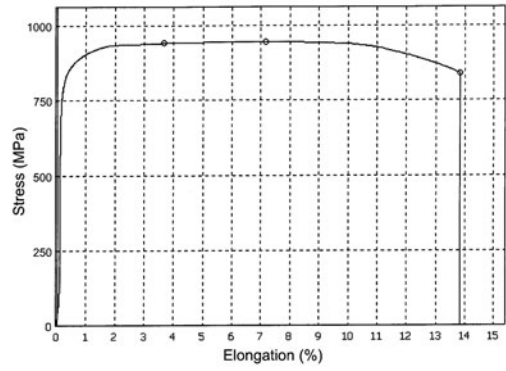
**3. Testing Conditions.** In this study, the most common type of fatigue test, Moore rotating beam under pure bending load, has been applied, the average stress being equal to zero; in other words, the stress range is twice the maximum stress [4].

The frequency of loading of test machine used is equal to 3500 rpm and the tests at 4 different levels of applied load 107.91, 117.72, 122.625, and 124.578 N are conducted; and the averaged experimental results obtained at each level are introduced as the number of cycles to fracture at that level; and based on it, the first component of the  $S-N$  curve (limited duration) of each of the analyzed coatings with a thickness of 13  $\mu\text{m}$  are obtained, as is shown in Fig. 5.

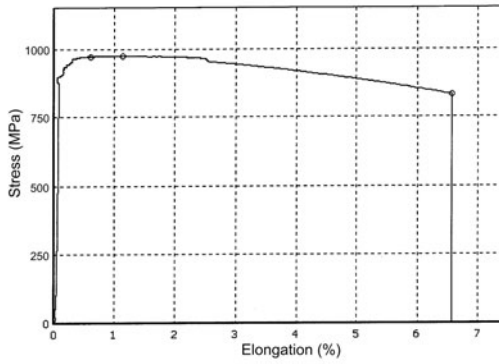
**4. Finite Element Analysis.** Fatigue analysis has traditionally been performed at a later stage of the design cycle. This is due to the fact that the loading information could only be derived from the direct measurement, which requires a prototype. Multibody dynamics is capable of predicting the component loads which enable a designer to undertake the fatigue assessment even before the prototype is fabricated. The purpose of analyzing a structure early in the design cycle is to reduce the development time and costs. This is achieved to determine the critical region of



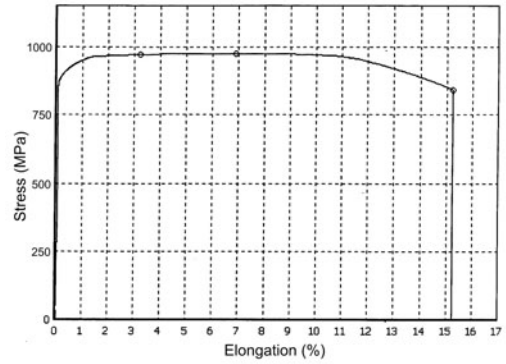
a



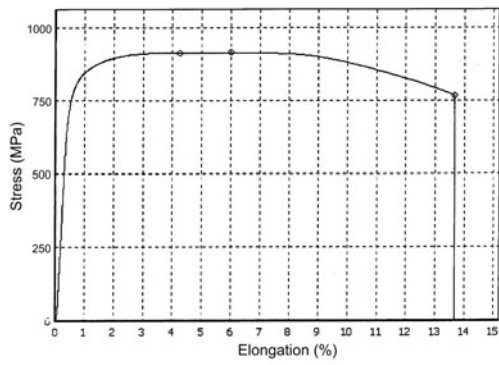
b



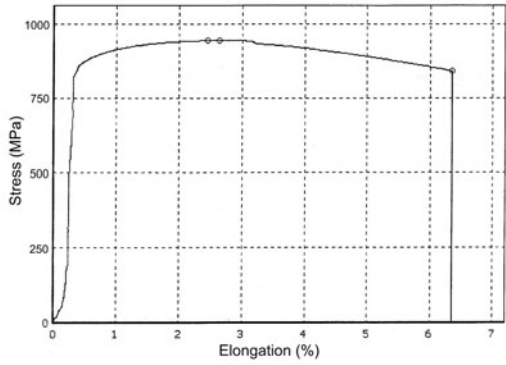
c



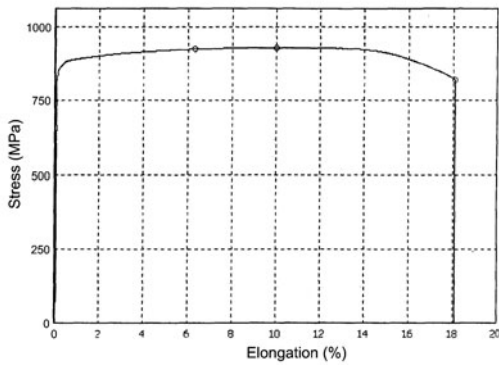
d



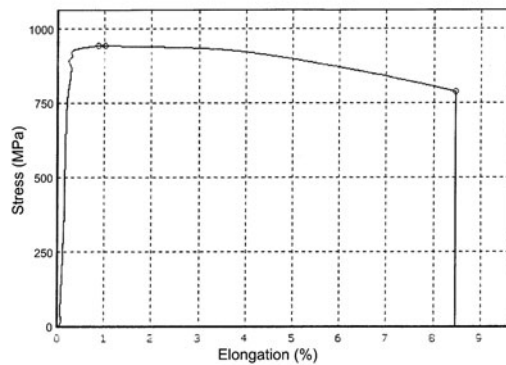
e



f



g



h

Fig. 2. Force curves in term of length extension of components with 13 (a–d) and 19  $\mu\text{m}$  (e–h) thicknesses: (a, e) trim chromium; (b, f) hardened chromium; (c, g) hardened nickel; (d, h) warm galvanization.

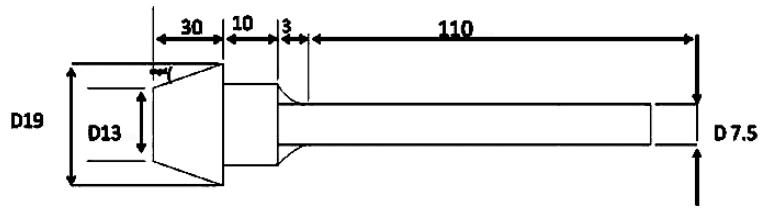


Fig. 3. A schematic of the fatigue test specimen [7]. (Dimensions in mm.)

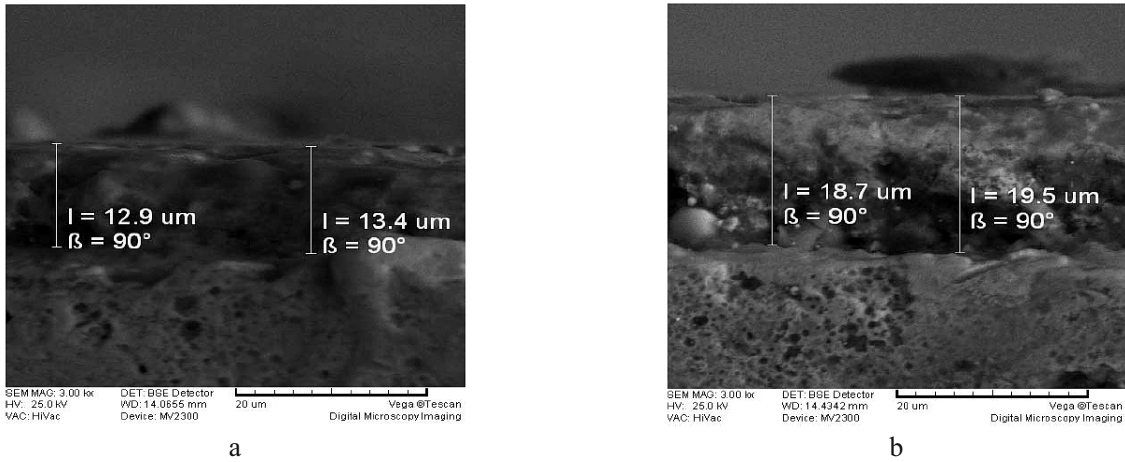


Fig. 4. Imaging surface of coating at components by SEM: (a) thickness of coating is 13  $\mu\text{m}$ ; (b) thickness of coating is 19  $\mu\text{m}$ .

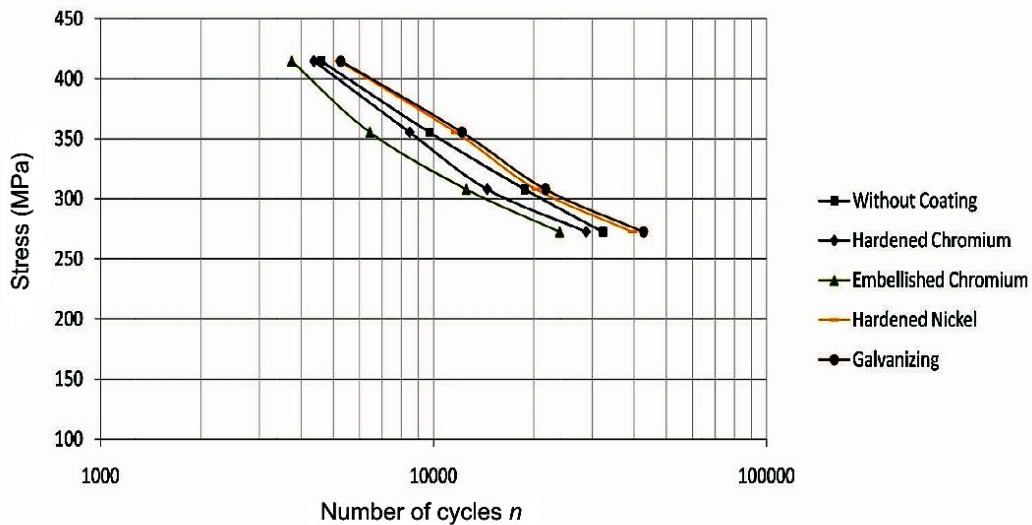


Fig. 5.  $S$ - $N$  curve of different coatings with the thickness of 13  $\mu\text{m}$  based on experimental data [6].

the structure and improving its design even before prototypes are produced and tested. The finite element method (FEM) based on fatigue analysis can be considered as a complete engineering analysis for the component. The fatigue life can be estimated for every element via FEM model, and the contour plots of life damage can be obtained. The geometry information is provided by the FEM result for each load case applied independently. The respective material properties are also provided for the applied fatigue analysis method. An integrated approach to fatigue life analysis combines the multibody dynamic analysis, FEM analysis, and the fatigue analysis into a consistent entity for the prediction of fatigue life of a component. A flowchart of the FEM-based fatigue analysis is shown in Fig. 6 [9].

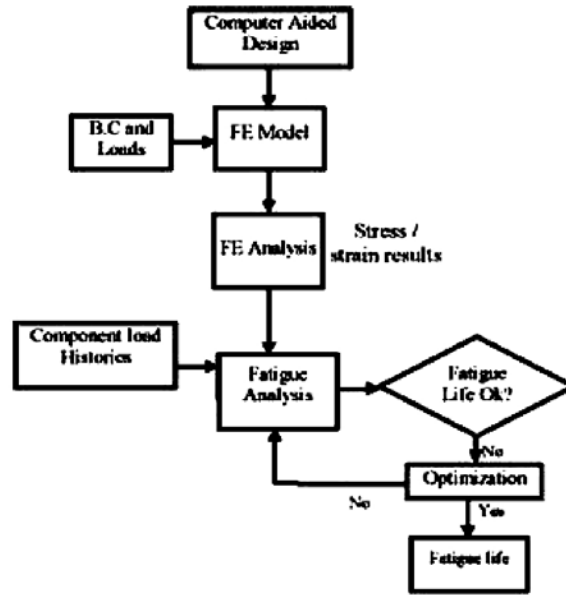


Fig. 6. The FEM-based fatigue analysis [9].

**4.1. Earlier Introduced Finite Element Model.** In the finite element model, which has been elaborated in 2011 within framework of the ANSYS software, two types of 3D elements, i.e., solid and shell ones, are used which are applied, respectively, for modeling the base steel, coating and the intermediate phase between them (having a smaller value thickness as compared to its length). In the new finite element model, including three separate phases, the base metal, coating and the interface between them are considered; whereas the mechanical properties of the interface, are treated as the average value of mechanical properties of the two adjoining phases [10–12].

In this model, by specifying the type of coating and the base metal, with this assumption, the mechanical properties of the intermediate phase can be easily assessed; while the thickness of intermediate phase is also considered to be equal to the length of the metallic bond between the atoms of the two adjoining phases.

**4.2. A New Finite Element Model.** The difference between the proposed model and earlier presented model is just in modeling the intermediate phase between the base metal and the coating. In the new model, a 3D linear spring element, which has the axial, bending and torsion stiffness, is used instead of shell element.

In the model, which describes 1/4 part of the component in cylindrical coordinates, the number of nodes at the outer surface of the base metal is considered equal to the number of nodes at the interior surface of coating, while each of the nodes of the two levels are linked together by a spring element.

In order to assess the spring stiffness, firstly, the axial, bending and torsion stiffness of a solid cylindrical beam (base metal model) and a hollow cylindrical beam (coating model or, in other words, the deposited component) are obtained through engineering formulas [13]:

$$K_r = \frac{AE}{L^3}, \quad (2)$$

$$K_{\varnothing} = \frac{IG}{L}, \quad (3)$$

$$K_{\theta} = EI. \quad (4)$$

Then, specifying the stiffness of the two phases of the model in each of the categories of loading, applying a specific load in the lab, and measuring the total changes and using the rule of total effects, we can obtain the ratio of unknown phase transformation from the total changes based on the Fig. 7; and then the stiffness of intermediate phase can be calculated.

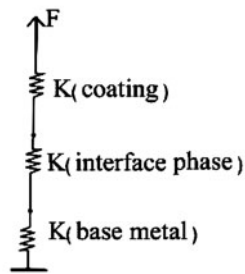


Fig. 7. A schematic of a solution for assessing the stiffness of the intermediate phase experimentally, based on stiffness of the other two phases.

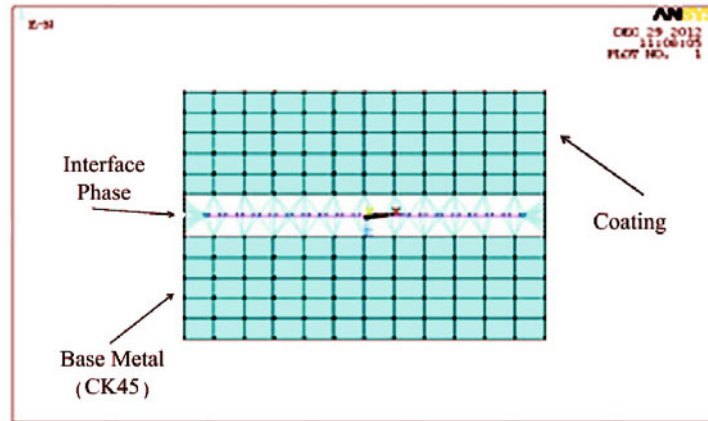


Fig. 8. FE model of the deposited components consisted of three independent phases in the ANSYS software.

One of the important issues that must be considered in the present finite element model is the length of a spring element used to model the intermediate phase between the base metal and the coating; so that specifying the two adjoining phases, the length of the metal bond of the atoms of the two adjoining phases is considered to be equal to the length of spring elements in the present model; as it is seen from the finite element model scheme depicted in Fig. 8.

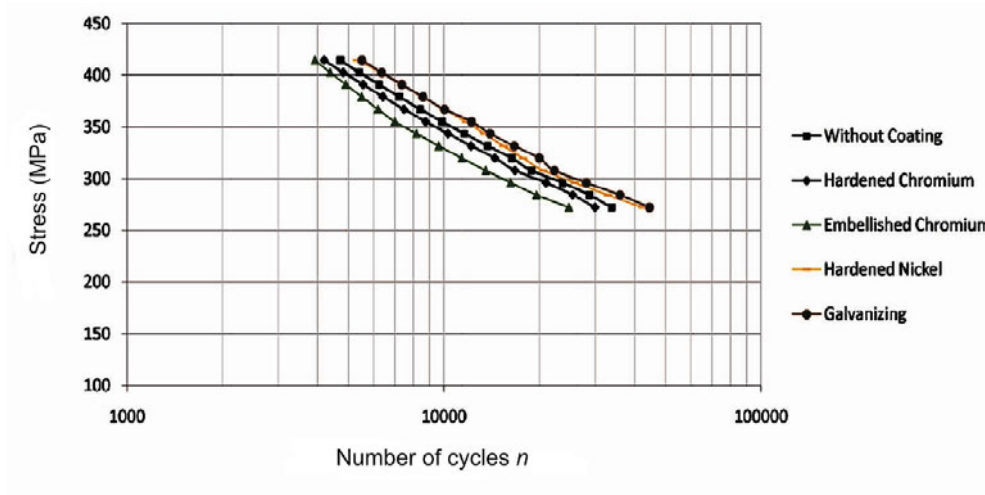
$S-N$  curves obtained from fatigue analysis via the ANSYS software using the new finite element model of the coated components with coatings of 13 and 19  $\mu\text{m}$  thickness values are depicted in Fig. 9.

The observed difference between the results obtained from finite element analysis and experimental data is attributed to application of a linear spring element, while for better approximation and closer fit one can use a nonlinear spring element, and moreover, the spring constants could also be calculated using different theories of the potential energy. However, in this research, linear spring element has been used, in order to reach acceptable results with the minimal computation efforts (increasing the speed of solving the equations) and simplification of governing equations (using linear terms instead of nonlinear terms).

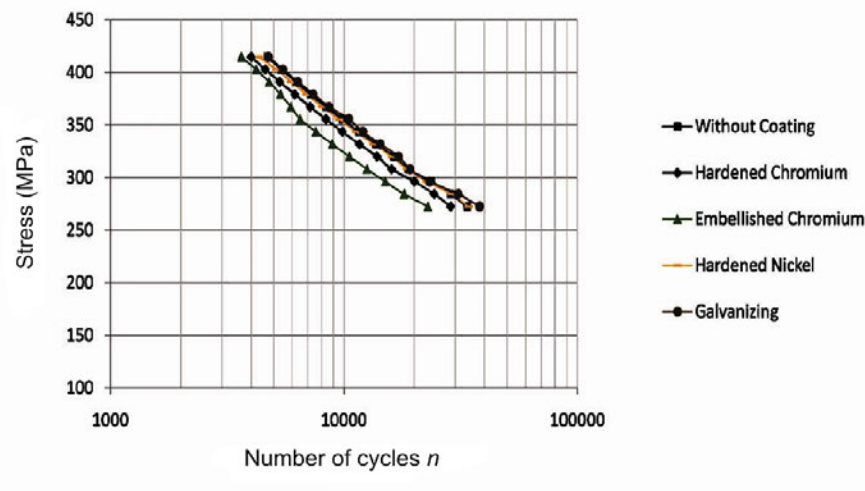
With account of the simplifications made, the results obtained from the experimental tests and finite element analysis (Figs. 6 and 7) indicate that, considering the environmental and operation conditions of components, a warm-galvanized coating with thickness less than 19  $\mu\text{m}$  is the most appropriate coating among the analyzed coatings. Consider the results of two finite element models and experimental data on the components with warm-galvanized coatings of 13  $\mu\text{m}$  in thickness, which are depicted in Fig. 10.

As it is seen from this plot, despite the fact that the results of a new finite element model and experimental data are different, their fit is improved, as compared to the earlier developed FEM model.

**5. The Effect of Coating Thicknesses on the Fatigue Life of Components.** As is seen from Fig. 9, with increased thickness the median between  $S-N$  curves of the coatings decreases, so that it may be possible to shift curves corresponding to different coatings by increasing their thickness and even change their position to each other.



a



b

Fig. 9.  $S-N$  curve obtained for components with a thickness of 13 (a) and 19  $\mu\text{m}$  (b) based on the extracted data of the software using the new FE model.

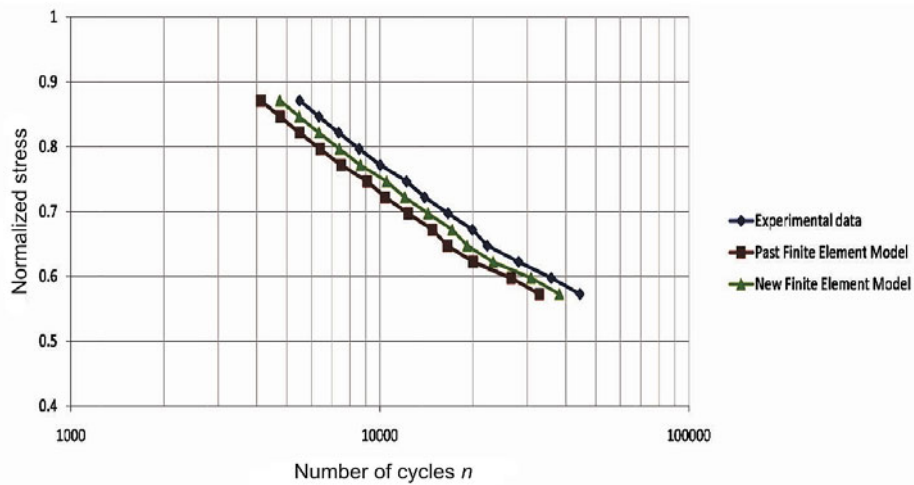


Fig. 10. Comparison of the  $S-N$  curve of the warm-galvanized coating with a thickness of 13  $\mu\text{m}$  through different methods.



TABLE 3. The Reduction of Fatigue Life of Components with Different Coatings for Increasing Thickness of 6  $\mu\text{m}$

Type of Coating	Reduction in fatigue life, %
Warm galvanizing	20.62
Hardened chromium	14.96
Embellished chromium	7.42
Hardened nickel	4.37

In this respect, data on the reduction of fatigue life of components, as a result of increasing thickness from 6  $\mu\text{m}$  to higher values are given in Table 3 for various coatings.

In the previous section, warm-galvanized coating was introduced as the most appropriate, but according to Table 3, the rate/speed of reduction of the fatigue life of components, as a result of equal increase in thickness of various coatings, is much higher for the warm-galvanized coating than for hardened chromium coating.

The highest amount of iron in the  $\gamma$ -layer of galvanized coating (closest coating layer to the base metal) may be treated as a metallurgical reason for embrittlement of cladding due to the increased thickness of the coating. As the coating thickness increases, the amount of iron in the  $\gamma$ -layer increases, and it leads to higher brittleness of the layer. Therefore, the rate of fatigue life reduction is a result of high increase in thickness.

According to the data from Table 3, the lowest rate of fatigue life reduction is observed in hardened chromium coating; in case where the coating thickness increases to a certain level, the best cladding is the warm-galvanized coating, and then the hardened chromium coating is the most appropriate cladding. Therefore, we have thickness limitation for the use of warm-galvanized coating; while beyond the limitation the hardened chromium coating is the best choice for applications under the analyzed operation conditions.

**Conclusions.** Considering the fact that the number of conducted tests exceeds than the standard number, the conclusions are quite reliable, and the galvanized coating is shown to be the most appropriate coating, being erosion-, corrosion-, and fatigue-resistant for very small values of coating thickness (13 and 19  $\mu\text{m}$ ) under the specified conditions.

For the analyzed loading conditions of the component, galvanized coating is the best than other coatings with small thickness values, while with increased thickness values, a galvanized coating becomes too brittle due to the high amount of iron in  $\gamma$ -layer, so that a hardened chrome coating should be used as the most appropriate coating, which is more resistant against erosion and corrosion under fatigue conditions.

However, the rate of reduction of the fatigue life under equal conditions of increasing the coating thickness is much higher for galvanized coatings, than for hardened chrome coatings. This is one of the reasons for using the hardened chrome coating in case of very high values of coating thickness.

More detailed calculations of this effect for galvanized coating require additional computation costs and efforts, and have yet to be performed.

Generally, hardened chrome coatings are used as the best protection against erosion and corrosion. However, in order to achieve the best performance and highest operational efficiency, the coating thickness should be determined based on the level of erosion and corrosion of the components, considering the operation conditions of the components, including the type and level of the applied load, parameters of corrosive environment, etc.

At last, the limited fatigue life and fatigue limit values should be assessed and, taking into account other parameters, such as cost, availability, etc., the most appropriate coating should be selected.

## REFERENCES

1. R. I. Stefener and H. A. Fuchs, *Metal Fatigue in Engineering*, Gilan University Publication (1998).
2. J. F. Luo, Y. J. Liu, and E. J. Berger, "Interfacial Stress analysis for multicoating systems using an advanced boundary element method," *Comput. Mech.*, **24**, 448–455 (2000).
3. C. Giummarra and H. R. Zonker, "Improving the fatigue response of aerospace structural joints," in: ICAF 2005 Proc., Hamburg, Germany (2005).

4. J. Lemaitre and R. Desmorat, *Engineering Damage Mechanics: Ductile, Creep, Fatigue and Brittle Fracture*, Springer, Heidelberg (2005).
5. Y. L. Lee, J. Pan, R. Hathaway, and M. Barkley, *Fatigue Testing and Analysis: Theory and Practice*, Elsevier, Boston (2005).
6. A. Arghavan, K. R. Kashyzadeh, and A. Amiri Asfarjani, "Investigating effect of industrial coatings on fatigue damage," *J. Appl. Mech. Mater.*, **87**, 230 (2011).
7. B. Khorshidi, *Strength of Material Lab*, University Book Publication (2004).
8. E. Besharat, *Metals Coating Engineering*, Tarrah Publication, Tehran (2005).
9. A. A. Asfarjani, S. Adibnazari, and K. R. Kashyzadeh, "Experimental and finite element analysis approach for fatigue of unidirectional fibrous composites," *J. Appl. Mech. Mater.*, **87**, 106 (2011).
10. H. Jahed Motlagh, *ANSYS*, Industry & Science University (2000).
11. D. A. Hancq, *Fatigue Analysis Using ANSYS*, ANSYS Inc. (2003).
12. R. Browell and A. Hancq, *Calculating and Displaying Fatigue Results* (2006).
13. A. Timoshenko, *Advanced Strength of Material*, Ayizh Publ. (2001).